GeoAmericas2020
4th PAN AMERICAN CONFERENCE ON GEOSYNTHETICS
26-29 APRIL 2020 • RIO DE JANEIRO • BRAZIL

Experimental Evaluation of Geocell Reinforcement Behavior using Transparent Soil Techniques

C.W.L. Nelsen, Hayward Baker, Inc., Odenton, Maryland, USA
J.G. Zornberg, Department of Civil and Environmental Engineering, The University of Texas at Austin, Austin, Texas, USA

ABSTRACT
Geocells are a growing type of geosynthetic product used in many applications, including the reinforcement of unbound granular materials for the construction of flexible pavements. Despite the burgeoning presence of geocells in the civil engineering industry, their acceptance and implementation by design engineers is limited by the lack of a clear design methodology. Although significant research has been conducted to quantify the performance of geocell-reinforced soil masses, there is no accepted design method for these structures. The Mechanistic-Empirical Pavement Design Guide (MEPDG) is a solid framework on which to base a geocell design method. The resilient modulus is the relevant design parameter that should be modified in the MEPDG for the design of pavement structures using geocells. However, a better understanding of the behavior and mechanisms that contribute to the performance of geocell-reinforced materials is necessary to develop theoretically-sound model. As such, the materials and equipment necessary to conduct a thorough analysis of geocells were conceived and developed as part of this study. This equipment is based on the transparent soil concept – transparent soils are two-part media consisting of solid particles and a saturating fluid with matching refractive indices. The large-scale equipment consists of a steel-framed tank with cast acrylic sides. Preliminary results indicate the equipment is adequate to validate the results of prior geocell experiments and provide novel insights into geocell behaviors and reinforcement mechanisms. Generalized results of this study, primarily the experience with transparent soils, can also be used for research into virtually any type of geosynthetic product.

1. INTRODUCTION

1.1 Motivation

Geocells are a growing type of geosynthetic product used in many applications, including the reinforcement of unbound granular materials for the construction of flexible pavements. Despite the burgeoning presence of geocells in the civil engineering industry, their acceptance and further implementation by design engineers is limited by the lack of a clear design methodology. The incorporation of theoretical reinforcement mechanisms into purely empirical design methodologies will improve the validity and accuracy of the methods. Recent advances in transparent soil technology have allowed some researchers to observe other complex soil-reinforcement interactions, especially in the context of geogrid reinforcement, (Peng and Zornberg 2016, 2017, Ezzein and Bathurst 2014, Bathurst and Ezzein 2015). Utilizing and scaling-up transparent soil techniques will allow for the direct observation and quantification of geocell reinforcement mechanisms in-situ – a novel use of transparent soil and a valuable perspective on geocell-reinforced soil behavior.

1.2 Objectives

The tangible objective of this research is to develop the equipment, techniques, and protocols necessary to implement transparent soil technology in experiments to observe, characterize, and quantify the separate reinforcement mechanisms that contribute to the improved performance of geocell-reinforced soil. In order to develop these experimental capabilities, it is also necessary to build a robust, theoretical framework that accounts for the soil reinforcement mechanisms on which to base a mechanistic design methodology. In the context of pavement design, this mechanistic design methodology will be compatible with the Mechanistic-Empirical Pavement Design Guide, or MEPDG, the developing standard of practice for flexible and rigid pavement design.

2. BACKGROUND

2.1 Theoretical Geocell Soil Improvement Mechanisms

As experimental laboratory and field work have been performed to understand the actual mechanisms involved in the performance, the understanding of geocell behavior has improved. It is widely accepted that geocells derive their improved performance from three main mechanisms: 1) the confinement effect, 2) the vertical stress dispersion effect, and 3) the tensioned membrane effect. The presence of these mechanisms as well as their relative contributions to the overall performance of the reinforced system depends on many factors such as the geocell geometry, the geocell-

reinforced system geometry, the loading on the system, and the native soil conditions. Additionally, the applicability of these mechanisms is also dependent on the framework of the design methodology and the imposed limit states.

The confinement effect has been generally accepted to involve providing additional or apparent "pseudo"-cohesion by the geocell to an otherwise unbound granular material (UGM). As the soil within an individual cell is loaded vertically, it tends to dilate and/or move laterally. This lateral movement is restricted by the geocell, the net effect of which is thought of as an induced or apparent cohesion. It has also been noted that a geocell mattress confines the soil vertically as well as laterally due to interface shear stresses between the infill and geocell sidewalls, (Pokharel, et al. 2010). The tendency to resist heaving around the loaded area may be an important mechanism in geocell-reinforced soil performance.

Analytical solutions for the stresses and deflections under a load of limited extent have shown that a material with a comparatively higher elastic modulus (i.e. stiffness) will distribute an applied load over a larger area than a less stiff material, (Foster and Ahlvin 1954). When subjected to a concentrated load, a geocell-reinforced soil mattress can act in this way, distributing the applied load over a wider area, thereby reducing the pressure applied to the underlying subgrade. This effect is known as vertical stress dispersion.

The tensioned membrane effect is a geosynthetic reinforcement mechanism that occurs frequently with planar reinforcement such as geogrids or geotextiles. For geocell-reinforced soil applications, the tensioned membrane effect occurs when significant vertical deformations (i.e. bending and/or rutting) occur causing the development of tensile stresses in the base of the geocell-reinforced layer. The vertical component of the tensile stresses is taken by the geocell itself thereby reducing the total amount of load transferred to the underlying subgrade, (Zhang, et al. 2010).

2.2 Mechanistic-Empirical Framework

2.2.1 The Mechanistic-Empirical Concept

The Mechanistic-Empirical concept couples 1) the mechanistic design procedure and 2) the empirical damage estimation and failure definition. This coupling is outlined in the Guide for Mechanistic-Empirical Design of New and Rehabilitated Pavement Structures (referred to hereinafter as the Design Guide). The mechanistic design procedure has three components: 1) the theory used to predict failure or distress, 2) the evaluation of material properties, and 3) the relationship between the magnitude of a particular distress parameter and the damage that should not be achieved to maintain the desired performance level. The theory used to predict distress in the Design Guide is a generalized multi-layered elastic theory discussed at length in Principles of Pavement Design, (Yoder and Witczak 1975). The empirical component refers to the damage models used to estimate the pavement damage (e.g. rutting, cracking) as a function of the stresses determined in the multi-layer elastic model.

2.2.2 Constitutive Relationship for Resilient Modulus, M_R

The material constitutive relationships used in the Design Guide are the models used to quantify the properties of the material components of a pavement structure (i.e. subgrade, base, and asphalt) over a range of conditions. The resilient modulus, M_R, is the design input for both base course and subgrade materials. As the base and subgrade are the layers most likely to be reinforced using geocells, they will be the focus of this section. The constitutive model for resilient modulus is often expressed as, Eq.1:

$$M_R = k_1 P_a \left(\frac{\theta}{P_a}\right)^{k_2} \left(\frac{\tau_{oct}}{P_a} + 1\right)^{k_3} \quad [8]$$

where:

M_R	=	resilient modulus, psi
θ	=	bulk stress = $\sigma_1 + \sigma_2 + \sigma_3$
σ_1	=	major principles stress
σ_2	=	intermediate principle stress = σ_3 for cylindrical tests
σ_3	=	minor principle stress/confining pressure
τ_{oct}	=	octahedral shear stress
	=	$\frac{1}{3}\sqrt{[(\sigma_1 - \sigma_2)^2 + (\sigma_1 - \sigma_3)^2 + (\sigma_2 - \sigma_3)^2]}$
P_a	=	atmospheric pressure (normalizing stress), ~14.7 psi
k_1, k_2, k_3	=	regression constants

The regression constants, k_1, k_2, and k_3, are determined from a linear or nonlinear regression analysis to fit the model to the M_R data generated in the lab. The coefficient, k_1, is proportional to the elastic modulus of the material, and as such the values of k_1 should be positive since the resilient modulus can never be a negative value. The first exponent, k_2, is

related to the bulk stress. An increasing bulk stress should stiffen the material resulting in a higher resilient modulus, so k_2 should also be positive. The second exponent, k_3, is related to the octahedral shear stress. Increasing shear stresses will soften the material, so k_3 should be negative. These three values, k_1, k_2, and k_3, are the actual input values for the mechanistic-empirical design process, not the resilient modulus itself as it is an extrinsic, stress-dependent property.

The inclusion of a geocell-reinforced soil layer into the mechanistic-empirical design process is the ultimate goal of this research trajectory. Using the MEPDG framework, the design of pavement structures using geocell reinforcement would be theoretically-sound and compatible with modern pavement design. As geocells are most commonly used to reinforce unbound aggregate materials, geocells would most effectively be used to reinforce the base course layer of a pavement structure, especially with the presence of weaker underlying subgrades. As mentioned in previous sections, the material constitutive relationship used for base course in mechanistic-empirical analyses is the resilient modulus. It follows that an analytical model for the reinforced resilient modulus of geocell-reinforced unbound aggregate materials would best fit into the mechanistic-empirical design approach.

2.3 Transparent Soil

As previously mentioned, transparent soils are two-part media consisting of a transparent particulate solid and a clear saturating fluid. If these two media have matching refractive indices, light will pass through the combined medium without reflecting or refracting off of any surfaces or facets giving outside observers the ability to visualize the movement of individual soil particles and the interaction between those particles and other objects. Fused quartz, also referred to as fused silica, is a transparent, granular soil surrogate that has been used in many recent geotechnical research applications, (Ferreira 2013, Ferreira and Zornberg 2015, Bathurst and Ezzein 2015, Peng and Zornberg 2016, 2017). Because of the application of geocells in the reinforcement of unbound aggregate bases, fused quartz is an ideal material to use for transparent soil evaluations of geocell-reinforcement mechanisms and behaviors.

The first application of transparent soil is the direct observation and qualitative characterization of soil-reinforcement interaction. In experiments with normal soil and careful exhumation procedures, the post-failure, post-test stage of in-situ conditions can be observed in some geotechnical experiments. Unlike those typical geotechnical experiments, a transparent medium allows for the visualization of material in-situ during every stage of loading. The observation of non-transparent objects acting on the transparent soil, such as cone penetrometers, geogrid reinforcement, and projectiles, allows for previously hidden phenomena to be revealed.

The next step beyond the direct observation of non-transparent objects acting upon the transparent soil is the observation of the motion of individual particles in response to perturbation. To this end, opaque soil particles have been used to track the displacement of individual soil particles within a transparent fused quartz soil mass, (Ferreira and Zornberg 2015). Planar lasers have also been used to illuminate individual planes of transparent soil particles within a transparent soil mass, either to take advantage of reflections off of individual fused quartz particles or to better illuminate the reflective seeding particles. This technique, when used appropriately, yields measurements with higher precision and resolution for displacement and strain contour maps than the use of opaque seeding particles due to the full-field illumination. Digital Image Correlation, DIC, is a common pattern recognition technique used frequently in association with transparent soil applications, (Iskander et al. 2015, Ganiyu et al. 2016).

3. MATERIALS AND EQUIPMENT

3.1 Materials

3.1.1 Geocell Test Sections

Geocell test sections manufactured from three different materials were obtained for this study. The first variety is a textured HDPE geocell, a typical material for commercially-available products. In order to take full advantage of the transparent soil capabilities, a transparent PVC geocell developed by Strata Systems, Inc. was obtained. A third variety of geocells, an untextured HDPE geocell, was also obtained to account for the contribution of side-wall texturing on the performance of geocell reinforcement. The full test section size was selected to fit into a 1219 mm x 1219 mm (48 in x 48 in) square plan area. This resulted in a full-sized test section consisting of a 4x4 matrix of cells, Figure 1 (left). The ½ and ¼ fractional cell size test sections consist of 8x8 and 16x16 matrices of cells of the corresponding size.

The test sections were custom-made in a variety of sizes for use in the proposed parametric study. The weld-spacing and h/d_e selections were based on a commercial geocell product with nominal expanded cell dimensions of 259 mm x 224 mm and standard available height-to-equivalent diameter (h/d_e) ratios of 1.0, 1.3, 1.9, and 2.6. Fractional sizes were selected in order to determine the effect of footing width to cell diameter (B/d_e) ratios. The (h/d_e) ratios were selected to be less than the standard ratios in an attempt to promote exaggerated failure mechanisms, in particular the tensioned

membrane effect. Three different weld spacings were used (356 mm, 178 mm, and 89 mm) with three (h/d_e) ratios (0.4, 0.8, and 1.6). As such, each fractional size of test section had three cell depths corresponding to the three standard aspect ratios.

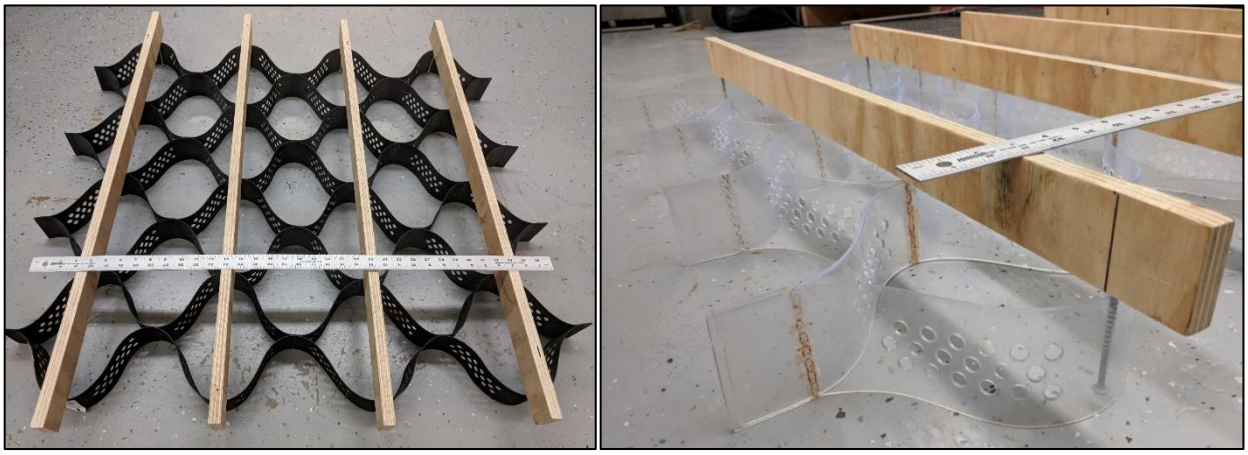

Figure 1. Fully expanded $HDPE_t$ GC 1-150 (left) vs. PVC GC 1-150 up close (right)

3.1.2 Transparent Soil

This study is one of, if not the, largest transparent soil experiments by volume ever conducted. As such, a very large quantity of fused quartz had to be sourced and processed into a usable product. Certain overseas manufacturers, mainly in China, can provide processed fused quartz particles in a range of grain size distributions, but due to the large quantity required the cost was prohibitive. Instead, a specialized glass producer, Heraeus Quarzglas was found with a facility in Austin, Texas. Heraeus manufactures a wide range of optical glass products for many applications including semi-conductor and solar panel manufacturing as well as many optical applications. The company has multiple product lines of fused quartz and fused silica with well-defined parameters and tolerances. Heraeus was able to supply scrap fused quartz tubes and other pieces in large quantities.

The scrap material obtained from Heraeus had to be crushed, cleaned, and sieved to create a suitable granular soil surrogate. The target grain size distribution for the crushed fused quartz was based on a truncated AASHTO #8 aggregate, with no particles passing a #8 sieve (2.36 mm) and no particles retained on a 3/8" sieve (9.5 mm), with a uniformity coefficient, C_u = 1.5, coefficient of curvature, C_c = 1.0, and USCS classification of GP, poorly-graded gravel. This target gradation was selected because similar aggregates and previous transparent soil batches have been used in geogrid pullout testing, (Peng and Zornberg 2016, 2017), and it is representative of typical unbound granular materials reinforced with geocells.

The final product after sieving and rinsing had a grain size distribution with slightly more particles passing a #8 sieve than originally desired, approximately 6%. The final gradation had a uniformity coefficient, C_u = 2.2, coefficient of curvature, C_c = 0.8, and USCS classification of SP, poorly-graded sand with gravel. This was determined to still be representative of soil types typically reinforced with geocells for pavement construction. Other typical geotechnical properties of fused quartz can be found in Peng and Zornberg 2016. Note that these values were determined for a different batch of fused quartz with a slightly finer grain size distribution, but it is assumed that the properties are nominally the same.

The saturating fluid selected for this large-scale application is based on the prior experience with transparent soils, (Ezzein and Bathurst 2011, Peng and Zornberg 2016). The crucial property to create a transparent soil is the refractive index, n, which is simply defined as the ratio between the speed of light passing through a vacuum and the speed of light passing through the material. The refractive index of fused quartz is well-defined, ~1.4586 at a reference wavelength of 589 nm, so the refractive index of the saturating fluid must match this value as closely as possible. Petro-Canada produces two white (clear) mineral oils, Puretol 7 Special and Paraflex HT4, that have refractive indices above and below the refractive index of fused quartz, 1.4635 and 1.4532, respectively. Because these two oils are miscible, they can be used to create a mixture with a refractive index approximated by a weighted average of the refractive indices by volume. A mixture ratio of 52% Puretol 7 Special and 48% Paraflex HT4 was found to be adequate for small-scale transparent soil applications, (Peng and Zornberg 2016).

3.2 Equipment

3.2.1 Large-Scale Transparent Soil Apparatus

The purpose of developing a large-scale transparent soil apparatus (LSTSA) was to test geocell-reinforced soil masses at the scale used in the field, while also utilizing the transparent soil techniques already employed for the characterization of geosynthetic-soil interaction mechanisms on smaller scales. As mentioned in previous sections, this study's focus is on the application of geocells for pavement design and the resistance of traffic loading. In order to visualize the mechanisms at work in a geocell-reinforced soil mass under traffic loading, a plate load test framework was adopted and based on ASTM D 1196-12 – The Standard Test Method for Nonrepetitive Static Plate Load Tests of Soils and Flexible Pavement Components.

The designated geocell test sections are based on 4x4 section a typical commercial geocell product with nominal-expanded cell dimensions 259 mm (10.2") x 224 mm (8.8") leading to overall test section dimensions 1,036 mm (40.8") x 896 mm (35.3"). The proposed transparent soil testing procedures necessitate fully-transparent side walls for the visualization of vertical soil particle movements and the bending and/or settlement of the geocell-reinforced section. In addition to transparent sidewalls, a transparent base panel is also required to enable to visualization of lateral soil particle movements and the expansion and/or contraction of individual geocells. The entire tank is elevated on a steel frame to facilitate the placement of a digital camera beneath the apparatus with a sufficient focal distance to capture the entire plan area. A rigid steel reaction frame was necessary for the application of the vertical load. The 3D model and assembled LSTSA are depicted in Figure 2. The LSTSA also includes a pneumatic loading system comprised of a pneumatic piston which can provide a theoretical maximum load of ~2,700 lbs with the available air pressure, the circular footing, and a 5,000-lb load cell.

Figure 2. Depiction of the 3D LSTSA Model (left) and the assembled LSTSA with 55-gal drums for scale (right)

3.2.2 Data Acquisition System and Sensors

In order to 1) validate the results of DIC procedures, 2) have a real-time indication of footing displacement during testing, and 3) directly compare results to previous geocell experiments, it was determined that physical displacement measurements were also required. Based on previous experience, UniMeasure LX-PA linear position transducers were selected for this purpose. These sensors are low cost, compact, and suitable for light- to moderate-duty applications. These sensors were used to measure vertical footing displacement as well as heave and/or settlement of the soil surface adjacent to the footing. Sensor mounting beams fabricated from lengths of ½"-square aluminum were used to secure the sensors in position above the footing and soil surface. In order to compensate for the nominal tension in the draw wires, steel hanging weights were made to rest on the soil surface with minimal influence on the heave/settlement response

during loading. A National Instruments Compact Data Acquisition System (cDAQ) was configured to measure and record the signals from the load cell and displacement sensors.

3.2.3 Optical and Image-Capture System

In anticipation of unique opportunities to observe and quantify soil-reinforcement interactions within the transparent soil, a DSLR camera and planar laser system was developed based on the system developed by Dr. Xin Peng, (Peng and Zornberg 2016). The system consists of a Nikon D5200 DSLR camera and a World Star Tech Compact Laser Controller. The planar laser illuminates a single plane of fused quartz particles within the transparent soil mass as depicted below in Figure 3. The DIC analysis procedure works best with a consistent texture as individual pixel clusters are identified in sequential images to develop a full-field displacement contour map. In this respect, the high contrast between the illuminated particle boundaries and darkened interiors is ideal for DIC analysis.

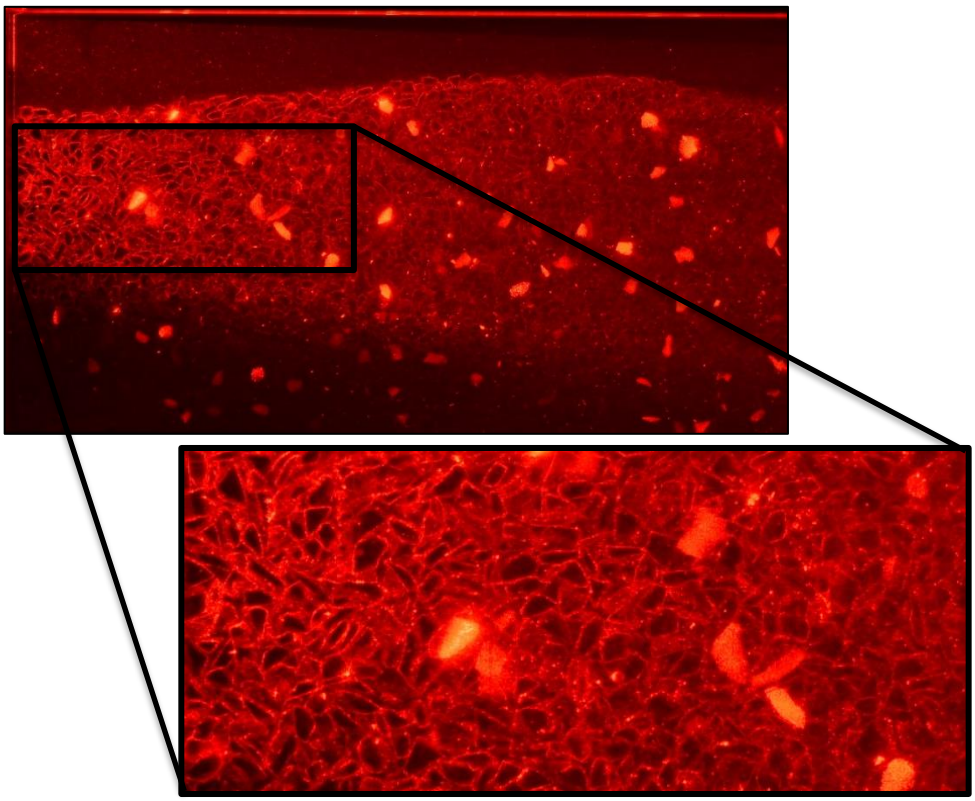

Figure 3. Laser-illuminated plane of fused quartz particles in a transparent soil mass

4. TYPICAL LARGE-SCALE TRANSPARENT SOIL APPARATUS RESULTS

A total of four full-scale tests were completed to verify the operation and preliminary capabilities of the LSTSA. Initially, one unreinforced test and one geocell-reinforced test were planned, but complications required repeats of both the unreinforced and reinforced tests. For brevity, only the 2nd set of tests will be discussed in the following sections. The prescribed loading sequence for all tests consisted of 50-lb load increments applied at approximately 1.5-min intervals. This loading sequence was maintained until the piston reached its full stroke.

4.1 Test Setup

In general, all tests were constructed of 8 lifts placed and compacted in a dry condition to approximately 85 pcf. Displacement sensors were placed in identical layouts between unreinforced and reinforced trials; a minor change was implemented between the first and second pair of tests to allow for transparent soil observation from a different angle. The dry soil mass was saturated with mineral oil after sensor setup was completed. In the case of the reinforced test, the geocell was placed in the 7th lift with its base approximately 14” above the base of the LSTSA tank. $HDPE_t$ GC 1-150 test sections were used for both tests, so the top of the geocell layer reached approximately 17” leaving another 0.5” for a

cover layer. It should be noted that the geocell test sections were filled and leveled, but not immediately compacted. The final compaction was performed after the placement of the cover layer to prevent damage to the geocell itself.

The displacement sensors were laid out in such a way as to capture a full profile of soil surface displacement in line with the center of the footing and observe whether or not the geocell reinforcement behaves differently on its perpendicular axes. Eight sensors were available to measure soil surface heave and/or settlement. Six of these sensors, referred to hereinafter as the main beam sensors were laid out along the centerline of the footing with three on each side. The closest sensors to the footing were 4" from the edge of the footing to the center of their hanging weight. The middle and furthest sensors were spaced 4" on-center. The remaining two sensors were placed in the same position relative to the footing as the two closest sensors on the main beam, but on the perpendicular axis. This layout is depicted on and unreinforced test bed in Figure 4.

Figure 4. Complete sensor layout on an unreinforced test bed

4.2 Load Versus Footing Displacement

The load-displacement response of the footing for both tests are presented in Figure 5 as bearing pressure (applied load / footing area) versus footing settlement ratio (footing diameter / displacement). The bearing capacity for this test can be defined as the pressure at which the first major change in displacement occurred, approximately 2 psi for the unreinforced case and 5 psi for reinforced case. Because of the load-controlled condition and resultant failure mechanisms, these results are difficult to compare with classical bearing capacity theories. An alternative failure criterion could be the load at which the footing reached a specific footing settlement ratio, say 10%. Using this definition, the unreinforced soil mass failed at ~19 psi and the reinforced soil mass failed at ~22 psi.

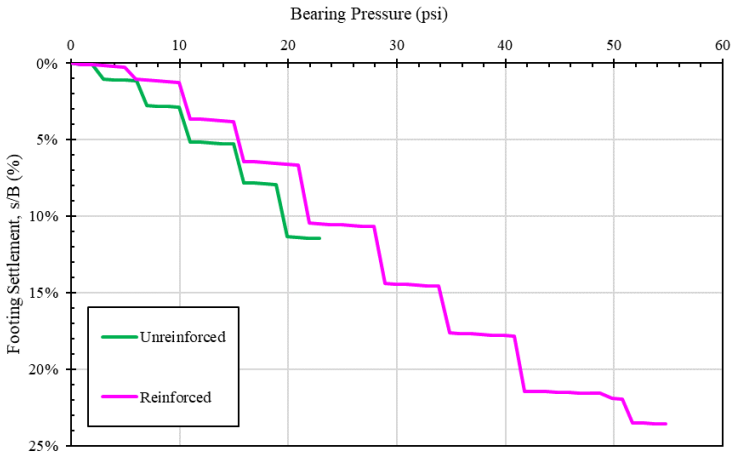

Figure 5. Bearing pressure vs settlement responses of both tests

4.3 Soil Surface Profiles

The displacement of the footing and soil surface, as measured by the average footing displacement and the six sensors on the main beam, can be used to create soil surface profiles at each increment of load, Figure 6. The behavior of the soil surface is indicative of the behavior of the unreinforced and the geocell-reinforced soil masses. The soil surface profiles indicate that the soil adjacent to the footing heaves up significantly as the footing is pushed downward. In the unreinforced case, the adjacent soil heaves ~0.2" by the end of the test when the footing displacement is ~0.9". The soil surface profile from the reinforced test reveals that the maximum heave experienced by the soil surface during the reinforced test was only 0.1", significantly less than the unreinforced test, although the reinforced soil surface profile suggests a wider generalized failure pattern and localized settlement within 4" of the footing perimeter.

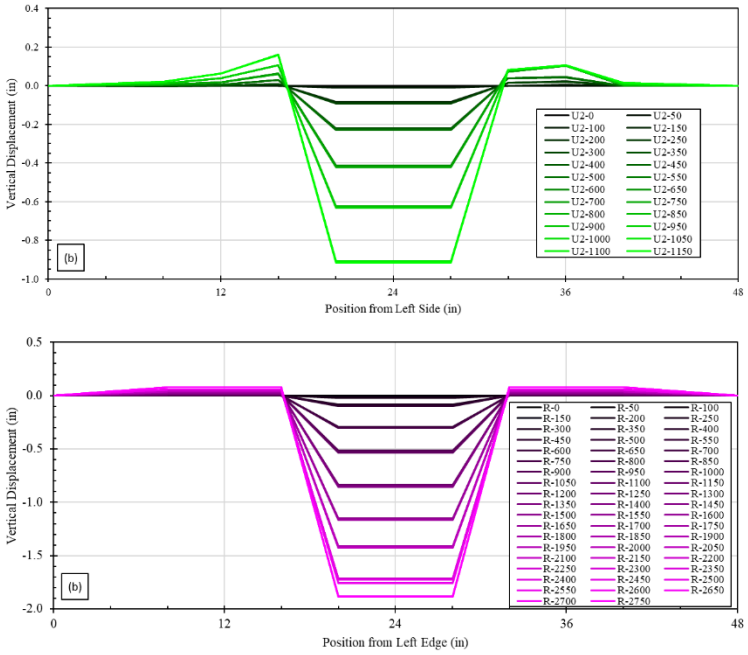

Figure 6. Soil surface profiles from the unreinforced test (top) and reinforced test (bottom)

Looking at the results depicted in Table 1, the reinforced soil mass performed substantially better. The first major displacement occurred at 5 psi during the reinforced test, while the same displacement occurred at only 2 psi during the unreinforced test. Additionally, the bearing pressure at a 10% settlement ratio was 3 psi greater for the reinforced case. Finally, the soil surface heave adjacent to the footing was only 0.1" at the end of the reinforced test, while it exceeded 0.3" by the end of the unreinforced test.

Table 1. Summary of physical measurement results of all four tests

Test Result	Unreinforced	Reinforced
Bearing Capacity @ First Major Disp.	2 psi	5 psi
Bearing Pressure @ s/B = 10%	19 psi	22 psi
Maximum Applied Pressure	23 psi	55 psi
Maximum Footing Settlement	12%	23%
Maximum Soil Surface Heave	0.3"	0.1"

4.4 Laser Plane Capabilities

Additional effort is required to reach a transparent soil quality adequate to observe full-field soil particle displacements on the centerline beneath the footing. However, it was found that with the current capabilities a laser plane illuminating a localized region of soil directly adjacent to the footing from an angled position above the soil surface could be captured

with a camera positioned similarly but perpendicular to the laser plane. An image depicting this set up is provided in Figure 7.

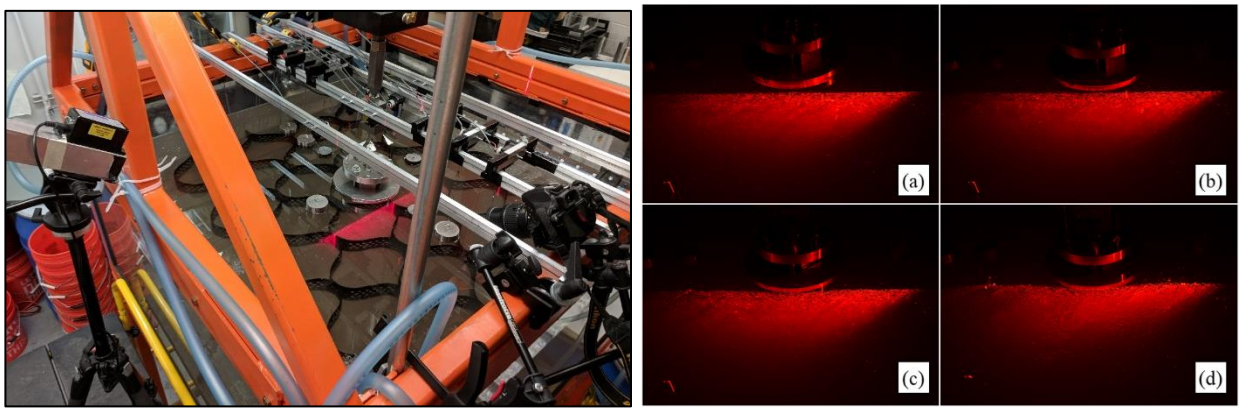

Figure 7. Optical system positioned to capture soil particle displacement (left) and selected images (right)

Images were taken from this camera position after every load increment and after any significant footing displacement event. Example images taken at various load increments during the unreinforced test demonstrate the potential to visualize and quantify soil particle displacements in this region. However, no DIC analysis was conducted on the images from any test at the time of writing. DIC analysis would be complicated by a number of factors including: 1) distorted perspective due to the refraction through the oil surface, 2) soil particle movement perpendicular to the laser plane, and 3) soil particles breaking the oil surface due to significant heave during later test stages that blurs particle boundaries.

5. CONCLUSIONS

The goal of this research is to develop the equipment, techniques, and protocols necessary to implement transparent soil technology in experiments to observe, characterize, and quantify the separate reinforcement mechanisms that contribute to the improved performance of geocell-reinforced soil. During the course of this research, the materials and equipment necessary to conduct a novel and comprehensive parametric evaluation of geocell-reinforced soil were developed and tested. During the development and initial testing performed with this equipment, the follow conclusions were made:

- Transparent soil is a useful technique to visualize and quantify soil-reinforcement interaction on a small scale with very high resolution and precision. However, scaling up the transparent soil concept to properly test geocell-reinforced soil masses exaggerates some existing challenges (material processing and handling, visualization and lighting procedures) and presents new difficulties (cloudy/non-transparent appearance at large depths, refractive index matching).
- The LSTSA is capable of testing geocell test sections to failure and making a number of typical physical measurements such as applied load, vertical footing displacement, and displacement of the geocell test section and adjacent soil mass. These measurements can be used for direct comparison to previous experimental campaigns as well as validate the results of transparent soil techniques in later testing.
- The results of the initial tests indicate that geocell reinforcement does improve the bearing capacity and, to a lesser extent, overall stiffness of unbound granular materials. However, the limitations of the loading system make comparisons to theoretical bearing capacity theories and the identification of true “failure” difficult.
- The reinforced tests showed less overall heave on the soil surface adjacent to the footing and even some settlement very close to the footing. The settlement was observed, not measured, as it occurred closer to the footing than the closest soil surface displacement sensor (within 4” of the edge of the footing). The hanging weights closest to the surface were clearly tilting in towards the footing at the end of the test despite the recording that indicated an overall heave at the 4”-mark. Laser plane illuminated and DIC would be able to provide much higher resolution soil surface profiles throughout the test.
- A direct comparison of the unreinforced test and reinforced test reveals that GC 1-150 test section improves the performance of the soil mass in terms of bearing pressure at which the first major displacement occurred, the bearing pressure at a settlement ratio of 10%, and the ultimate heave of the soil surface adjacent to the footing.

ACKNOWLEDGEMENTS

I would like to acknowledge the following individuals and organizations for contributing to and supporting this research: The University of Texas at Austin Geotechnical Engineering Faculty, especially to my advisor, Professor Jorge Zornberg, The Jack and Carrie Howe Endowed Graduate Fellowship in Engineering, Dr. Amr Morsy, Dr. Xin Peng, Federico Castro, Dr. Gregório Araújo, Dr. Yuri Costa, Phil Tomlin, Lamont Prosser, Alejandro Marez, Luis, Carlos, Sam, Henry, and Mario, Heraeus Quarzglas, Bosque County Recycling Center, especially Dianne Bernhardt, and Joe Friedrichsen.

REFERENCES

ASTM D 1196. Standard Test Method for Nonrepetitive Static Plate Load Tests of Soils and Flexible Pavement Components, for Use in Evaluation and Design of Airport and Highway Pavements, *American Society for Testing and Materials*, West Conshohocken, Pennsylvania, USA.

ARA, Inc., ERES Consultants Division. 2004. Guide for Mechanistic-Empirical Design of New and Rehabilitated Pavement Structures. Final Report, National Cooperative Highway Research Program, Transportation Research Board, National Research Council.

Bathurst, R. J., and F. M. Ezzein. 2015. "Geogrid and soil displacement observations during pullout using a transparent granular soil." Geotechnical Testing Journal 673-685.

Ezzein, F. M., and R. J. Bathurst. 2014. "A new approach to evaluate soil-geosynthetic interaction using a novel pullout test apparatus and transparent granular soil." Geotextiles and Geomembranes 246-255.

Ezzein, F. M., and R. J. Bathurst. 2011. "A transparent sand for geotechnical laboratory modeling." Geotechnical Testing Journal 590-601.

Ferreira, J. A. Z. 2013. Evaluation of soil-geogrid interaction at different load levels using pullout tests and transparent soil. PhD Thesis, Austin, TX: The University of Texas at Austin.

Ferreira, J. A. Z., and J. G. Zornberg. 2015. "A transparent pullout testing device for 3D evaluation of soil-geogrid interaction." Geotechnical Testing Journal 686-706.

Foster, C. R., and R. G. Ahlvin. 1954. "Stresses and deflections induced by a uniform circular load." Thirty-Third Annual Meeting of the Highway Research Board. Washington, D.D.: Highway Research Board. 467-470.

Ganiyu, A. A., A. S. A. Rashid, and M. H. Osman. 2016. "Utilisation of transparent synthetic soil surrogates in geotechincal physical models: a review." Journal of Rock Mechanics and Geotechnical Engineering 568-576.

Iskander, M., R. J. Bathurst, and M. Omidvar. 2015. "Past, present, and future of transparent soils." Geotechnical Testing Journal 557-573.

Peng, X., and J. G. Zornberg. 2017. "Evaluation of load transfer in geogrids for base stabilization using transparent soil." Transportation Geotechnics and Geoecology. Saint Petersburg, Russie: Elsevier. 307-314.

Peng, X., and J. G. Zornberg. 2016. "Evaluation of load transfer in triaxial geogrids using transparent soil." GeoAmericas 2016, 3rd Pan-American Conference on Geosynthetics. Miami Beach, Florida: International Geosynthetics Society. 1520-1531.

Pokharel, S. K. 2010. Experimental study on geocell-reinforced bases under static and dynamic loading. Dissertation, Lawrence: The University of Kansas.

Yoder, E. J., and M. W. Witczak. 1975. Principles of Pavement Design. New York: Wiley.

Zhang, L., M. Zhou, C. Shi, and H. Zhou. 2010. "Bearing capacity of geocell reinforcement in embankment engineering." Geotextiles and Geomembranes 475-482.